Article

Tribological Behavior of Doped DLC Coatings in the Presence of Ionic Liquid Additive under Different Lubrication Regimes

Mohammadamin Sadeghi [1], Takeru Omiya [1,2], Filipe Fernandes [1,2,3], Luís Vilhena [1], Amilcar Ramalho [1] and Fábio Ferreira [1,2,4,*]

1 Department of Mechanical Engineering, CEMMPRE, ARISE, University of Coimbra, Rua Luís Reis Santos, 3030-788 Coimbra, Portugal; masadeghiedu@gmail.com (M.S.); omiya1130@gmail.com (T.O.); filipe.fernandes@dem.uc.pt (F.F.); luis.vilhena@uc.pt (L.V.); amilcar.ramalho@dem.uc.pt (A.R.)
2 Laboratory for Wear, Testing & Materials, Instituto Pedro Nunes, Rua Pedro Nunes, 3030-199 Coimbra, Portugal
3 ISEP, Polytechnic of Porto, Rua Dr. António Bernardino de Almeida, 4249-015 Porto, Portugal
4 Walker Department of Mechanical Engineering, The University of Texas at Austin, Austin, TX 78712, USA
* Correspondence: fabio.ferreira@dem.uc.pt

Abstract: Diamond-like carbon (DLC) coatings are widely used in industries that require high durability and wear resistance, and low friction. The unique characteristics of DLC coatings allow for the possibility of creating adsorption sites for lubricant additives through the doping process. In this study, the combined use of europium-doped diamond-like carbon (Eu-DLC), gadolinium-doped diamond-like carbon (Gd-DLC), and pure DLC coatings and an ionic liquid (IL) additive, namely, trihexyltetradecylphosphonium bis (2-ethylhexyl) phosphate $[P_{66614}]$ [DEHP], with a 1 wt.% concentration in polyalphaolefin (PAO) 8 as a base lubricant was investigated. Higher hardness, higher thin-film adhesion, a higher ratio of hardness to elastic modulus, and a higher plastic deformation resistance factor were achieved with the Gd-DLC coating. The CoF of the Gd-DLC coating paired with the IL was superior compared to the other pairs in all lubrication regimes, and the pure DLC coating had a better performance than the Eu-DLC coating. The wear could not be quantified due to the low wear on the surface of the DLC coatings. The friction reduction demonstrates that tribological systems combining Gd-DLC thin films with an IL can be a potential candidate for future research and development efforts to reduce friction and increase the efficiency of moving parts in internal combustion engines, for instance.

Keywords: ionic liquid; doped DLC; lubrication regime; Stribeck curve; friction

1. Introduction

Modern industrial systems involve a variety of mechanical systems that have various moving components and, as a result, interacting surfaces. The ability of such machines to perform smoothly, consistently, and over an extended period depends heavily on how effectively wear and friction are managed across their multiple interacting surfaces [1]. Focusing on this issue, in our understanding, there has been significant progress in the basic mechanisms underlying tribological phenomena and the creation of a wide range of new materials, surface engineering techniques, lubricants, and other types of technical solutions [1]. In response to the increasing demand for considering environmental sustainability, various businesses have carefully been analyzing how industrial processes can be updated to achieve a more efficient and cleaner process [2].

Additives for lubricants are widely employed to enhance already existing qualities or to introduce extra tribological properties. They include chemical substances that can adhere to and/or interact with solid surfaces to form protective, low-shear-strength reaction layers (referred to as "tribofilms"), which are intended to lower wear and friction [2].

Furthermore, diamond-like carbon (DLC) thin films have been shown to have high hardness and wear resistance and a low friction coefficient (CoF) [3,4], and to be biocompatible. DLC thin films, one of the most promising categories of surface engineering solutions, have been the subject of many investigations, specifically in the automotive industry. The tribological behaviors of DLC films depend on external factors such as temperature, which results in various degrees of wear rates for the same film [5,6]. Several research projects have investigated the doping of DLC films with various metallic elements to further enhance their qualities and, primarily, to adjust some undesired traits, even beyond the good mechanical and tribological capabilities of currently available DLC coatings [4]. Usually, two categories of alloying materials are used to adjust the characteristics of DLC coatings: carbides (for instance, Ti, Cr, F, and W) and non-carbide formers (for example, Cu and Ag) [7–13].

Ti, Cr, W, Nb, Mo, and Zr as well as the non-carbide formers Ag, Cu, and Al have been investigated as doping choices to enable a reduction in the high internal residual stress and to enhance adhesion, thermal stability, corrosion resistance, and biocompatibility [2,9,11,14–17]. Tungsten is the most researched metallic element among those chosen for doping as a result of its potential to modify the tribological behavior of DLC under high temperatures [4,13].

Lanthanides (which include the Eu and Gd elements) are believed to have a positive effect on tribolayer formation when ionic liquids are used as additives because they show a high affinity for ILs [18,19]. On the one hand, DLC thin films that are doped with Eu or Gd at an atomic concentration between 1% and 3% exhibit the usual traits of un-doped DLC coatings, including a low specific wear rate (10^{-16} m^3/Nm) and high hardness (23 GPa) [4]. Nonetheless, if the doping elements possess a high atomic concentration in the doped DLC coating, the consequence can be detrimental to the film's characteristics [4].

Ionic liquids (ILs), among several solutions recommended as an addition to or equivalent of ZDDPs, have attracted a lot of attention from tribologists in recent years. An anion and an organic cation make up ILs, which are liquid salts with melting points under 100 °C [20,21]. Large organic molecules represent the majority of ILs' ions [22,23]. The majority of ILs do not have any metal components. Therefore, they react with metal substrates or resultant wear debris. This results in a metal-based film that is created by ILs. Usually, tribofilm compositions formed by ILs containing P are quite similar to those formed by ZDDPs [22].

Trihexyltetradecylphosphonium bis (2-ethylhexyl) phosphate [P$_{66614}$] [DEHP] was chosen for use in this study. It was synthesized using the method described in [24]. It is a prospective anti-wear lubricant addition for steel–cast iron contacts and was described in 2012 as having mutually miscible features in non-polar hydrocarbon lubricants [25,26]. Later investigations from a few different groups [27,28] confirmed its oil miscibility and showed efficient wear mitigation in lubricating steel–aluminum and steel–steel contacts, which strengthened the idea of employing [P$_{66614}$] [DEHP] as an anti-wear additive [24].

Milewsk et al. [29] investigated the tribological response of two ionic liquids using a ball-on-disc tribometer on an a-C: H-type diamond-like carbon coating under boundary lubrication conditions and reported that the smallest friction coefficient was found for the a-C: H-type DLC film and the ionic liquid acting as the lubricant.

Gonzalez et al. [30] assessed the performance of a Cr-DLC film and two types of ionic liquids as 1 wt.% additives to polyalphaolefin as the base oil. They reported that both ILs caused a friction drop.

The tribological interactions of three ILs and a tungsten-doped DLC thin film were investigated and [31,32] analysis showed that an adsorbed layer with a thickness of 0.75 nm formed on the W-DLC surface. Hence, the authors concluded that doping DLC thin films with tungsten (i.e., W-DLC) effectively enhances their reactivity with $[P_{4441}]^{+}$ $[DMP]^{-}$ − ILs, therefore improving their tribological properties.

Khanmohammadi et al. [2] analyzed two additive adsorption mechanisms dominating the tribological behavior of three types of DLC coatings (pure DLC, W-DLC, and Ag-DLC) in the presence of three groups of ILs and concluded that a triboelectrochemical activation

process for Ag-DLC coatings and an electron transfer mechanism for tungsten-doped DLC coatings led to an efficient drop in friction in the contact.

PAO 8 is a highly branched lubricant used in the automotive industry, and a few investigations have been carried out to improve its tribological performance in lubricating DLC coatings (DLC coatings are also widely used in the automotive industry due to their favorable tribological properties) [33–35]. On the other hand, even though previous investigations have shown that lanthanides, including Eu (europium) and Gd (gadolinium), have a high affinity for ILs and, in some cases, ILs have even been used for the recovery of rare-earth metals [18,19,36], their potential advantage for improving the tribological interaction between lanthanide-doped DLC thin films and ILs has not been thoroughly investigated. Therefore, in this study, the effect of doping DLC coatings with Eu and Gd (deposited using high-power impulse magnetron sputtering) on their tribological response to a newly developed IL (trihexyltetradecylphosphonium bis (2-ethylhexyl) phosphate [P_{66614}] [DEHP]) was studied by mixing the IL (as an additive) with PAO 8 as a base oil (1 wt.%) under various lubrication regimes by changing the speed of the rotating ring in a block-on-ring configuration at room temperature and comparing the results with the samples lubricated with the base oil (without additives), to show the advantage of the doping process on the tribological performance of the DLC coatings in the presence of an IL additive.

2. Materials and Methods

2.1. Preparation of Materials

The substrate for the DLC coatings was steel (AISI M2), with a diameter of 25 mm and a thickness of 4 mm, while the substrate for the morphological study of the coatings was silicon wafers [4], 20 × 20 mm. Abrasive grit papers with grit sizes of 240, 320, 400, 600, 800, and 1200 were used to grind the steel specimens. Diamond abrasive paste with particle sizes of 6 and 3 μm was employed for mirror polishing. All substrates were cleaned in 100% ethanol and acetone for a total of 15 min with a series of ultrasonic baths. The substrates were cleaned, and then before placing the samples inside the deposition chamber, silver glue was used to adhere them to the substrate holder and make them conductive [4].

2.2. Deposition Processes of Coatings

A DOMS (deep oscillation magnetron sputtering) power supply (HiPIMS Cyprium™ plasma generator, Zpulser Inc., Mansfield, MA, USA) was used to produce the coatings. The substrate holder rotated at a speed of 23.5 rev/min along the chamber's axis for all depositions, and the substrates were kept 80 mm away from the carbon and chromium targets. Targets composed of chromium (purity 99.99%) with a size of 150 mm by 150 mm and a thickness of 10 mm and pure graphite (purity 99.95%) were used to deposit the interlayers and DLC coatings, respectively. The carbon target, chromium target, and substrates were etched prior to all depositions. The graphite target was machined with circular grooves of 10 mm diameter and 2 mm depth to hold the doping pellets (Gd or Eu pellets) during the deposition process. For depositing pure DLC films, graphite pellets were employed to fill the round holes and standardize the target surface in the absence of doping pellets. To establish a base pressure of less than 3×10^{-4} Pa, two (a rotary and a turbomolecular) pump systems were used. To increase the DLC film's adherence to the substrates, two interlayers were coated prior to the final DLC thin film. A layer of Cr was applied first, followed by a layer of CrN [4]. Three stages made up the deposition process: etching the substrate and target, depositing the interlayer, and depositing the DLC-based coating. During the etching process, the carbon target was cleaned for 10 min using a direct current (DC) of 0.4 kV at 0.4 Pa of pressure. Then, a cleaning process was also performed on the chromium target for 10 min applying a power of 0.25 kW and a pressure of 0.35 Pa. Subsequently, the substrate was also cleaned. Figure 1 shows a schematic presentation of the coating process.
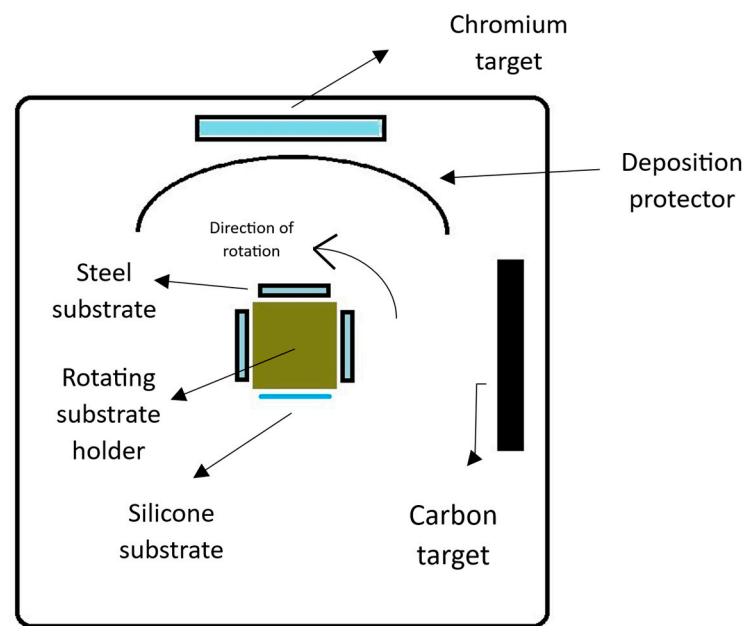
Figure 1. Schematic presentation of the coating process.

2.3. Lubricants

To clarify the role of the coatings, it was necessary to employ a basic lubricating oil that was free of additives and to later mix it with additives to investigate the tribological features of the thin films when exposed to an IL+ base lubricant. The hydrodynamic and mixed lubrication regimes in internal combustion engines dominate the contact between the piston ring and cylinder liner for the most part, but a boundary lubrication regime is frequently found at the top dead center of the stroke, which necessitates the implementation of coatings. Polyalphaolefin (PAO) 8 was selected as the base lubricating oil because it serves as the base oil for various commercial engines [34,37,38]. Trihexyltetradecylphosphonium bis (2-ethylhexyl) phosphate [P_{66614}] [DEHP] ionic liquid was used in this study. By combining 1 g of [P_{66614}] [DEHP] with 99 g of PAO 8 using an analytical balance, a lubricant with 1 wt.% of [P_{66614}] [DEHP] was created.

2.4. Characterization Analysis

Nano-indentation was implemented to determine the reduced Young modulus and hardness. A Berkovich diamond indenter was part of the nano-indenter (Micro Materials, Wrexham, UK). To ensure that the indentation depth was less than 10% of the coating thickness, a maximum load of 10 mN (typical settings in the CEMMPRE laboratory) was applied. For each sample, sixteen evaluations were carried out to determine the mean and standard deviation of the mechanical parameters [39,40].

The chemical content of the thin film was assessed using the SIAM platform based on Rutherford backscattering spectrometry (RBS) and elastic recoiling detection (ERD). The specimen was tilted at 70 degrees and exposed to an alpha beam examination at 2.3 MeV while collecting backscattered particles using a fixed detector (homemade, Namur, Belgium) positioned at 30 degrees from the incident beam path. Records of the elemental depth [41] were produced using DataFurnace to process the five spectra that were captured for each specimen [42]. SigmaCalc data were implemented to measure the cross-section functions, and the SRIM documents for the stopping power were used in these evaluations [43].

To assess the coating adhesion, an automatic scratch tester model (CSEM Revetest, Neuchâtel, Switzerland) was used with a Rockwell "C" diamond-tipped indenter having a spherical tip diameter of 100 μm. The scratch test was performed with a linear increase in the normal load from 0 to 60 N, and the test speed was set to 0.167 mm/s with a loading rate of 10 N/mm. Samples and the indenter were cleaned with ethanol before testing.

The adhesive properties of the coatings were quantified using an optical microscope, and the test was repeated three times for each sample in order to verify the consistency of the results.

The SV-100 A&D viscometer (A&D Weighing, Tokyo, Japan) was used to measure the viscosity–temperature–time parameters of the lubricant based on the tuning-fork vibration principle. The device was calibrated before performing measurements, and the container of the device was cleaned with ethanol and dried before starting the test.

The device used for the tribology testing was an in-house tribometer with a block-on-ring configuration, where the contact geometry was a rectangle. The laboratory setup included a power supply and controller, sample support, counter body, oil reservoir, and two force sensors (one for the normal force F_N and another for the tangential force F_f). According to Amontons' 1st law, the tangential force is directly proportional to the normal force, where the coefficient of proportionality (μ) is the coefficient of friction. The contact was kept lubricated by a reservoir of lubricant, fully flooded. As a counterpart, an AISI 3415 steel ring (often used for cylinder liners) with a diameter of 115 mm and width of 12 mm was used. The ring surface was polished with 2000 granulometry sandpaper to resemble the surfaces frequently employed in internal combustion engines [34]. Then, with the help of a profilometer, the surface roughness was measured. The applied normal load of 25 N was determined, according to Hertzian contact theory and considering the geometry of the block-on-ring contact and the internal combustion engine's working pressure range, which was assumed to be on the order of 40 MPa. Figure 2 shows a simple representation of the block-on-ring setup used in this work.
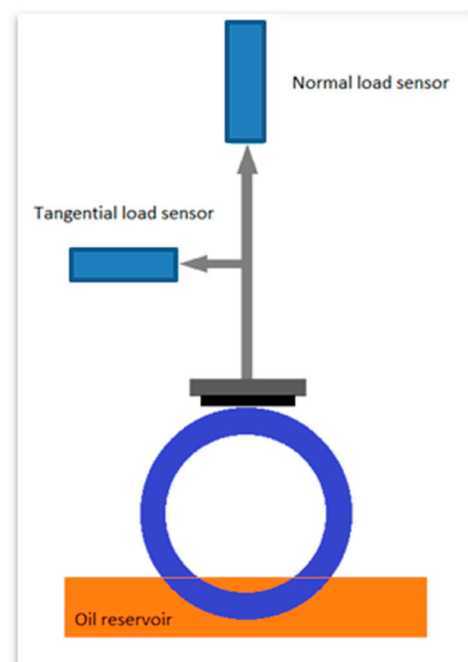
**Figure 2.** A simple representation of the block-on-ring setup.

Scanning Electron Microscopy-Energy Dispersive X-ray Spectroscopy (SEM-EDS) (Hitachi High-Tech, Tokyo, Japan) was used to identify dissimilar matters; therefore, in this research, it can be used to investigate the worn surface and the layers [44].

3. Results and Discussion

3.1. Hardness, Reduced Young Modulus, and Chemical Composition

The measurements showed that the Gd-DLC coating had a higher hardness than the Eu-DLC and pure DLC coatings, while in the case of Young's modulus, the Eu-DLC coating had the best performance (Figure 3). The sp^3 hybridization percentage in the

structure of the corresponding DLC coatings may explain this finding. DLC is primarily composed of two types of carbon bonds that are similar to those found in graphite (known as sp^2 hybridizations) and diamond (known as sp^3 hybridizations). DLCs are known for their exceptional hardness and high elastic modulus, although they also exhibit high internal stresses [45,46]. These characteristics are closely attributed to the proportion of sp^3 hybridizations present in the films. It is reported that the higher the sp^3 hybridization percentage and density, the higher the hardness and elastic modulus [4,13,47–50].
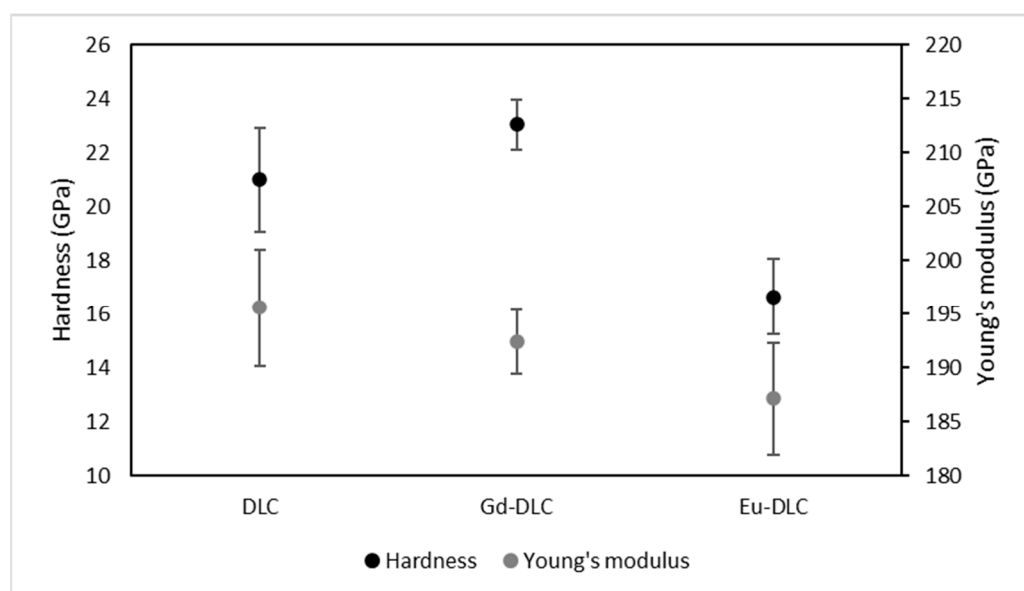
Figure 3. Hardness and Young's modulus of the DLC coatings.

Surfaces with greater hardness are more resistant to abrasive wear. Additionally, materials with a lower elastic modulus experience elastic deformation at a higher intensity. Therefore, the ratio of hardness to elastic modulus (H/E) and the plastic deformation resistance factor (H^3/E^2) have been discussed in the literature as good representatives for describing the mechanical characteristics of thin films [2,51,52].

The H/E and H^3/E^2 ratios of the thin films are presented in Table 1. The Gd-DLC film had the greatest H/E ratio, followed by the pure DLC and Eu-DLC films. This finding may indicate the advantages of a low elastic modulus and a comparatively greater hardness. The Gd-DLC coating had the greatest resistance against plastic deformation (H^3/E^2), followed by the pure DLC and Eu-DLC coatings. From the H^3/E^2 ratio, it can be inferred that greater hardness overweighs the elastic modulus in decreasing the intensity of plastic deformation [2].

Table 1. H, E, H/E, and H^3/E^2 values of the films.

| Coating	H (GPa)	E (GPa)	H/E	H^3/E^2
Pure DLC	20.992 ± 1.936	195.583 ± 5.391	0.107 ± 0.010	0.242 ± 0.050
Gd-DLC	23.047 ± 0.920	192.388 ± 2.981	0.120 ± 0.005	0.330 ± 0.024
Eu-DLC	16.649 ± 1.423	187.126 ± 5.149	0.089 ± 0.008	0.132 ± 0.020

Based on the results of the Rutherford backscattering spectrometry (RBS) and elastic recoiling detection (ERD) tests, both doped DLC coatings contained 1.7 at. % of the doped elements (Table 2). Previous research showed that increasing concentrations of Eu and Gd in doped DLC thin films affect the properties of the thin films in a negative trend [4]. For instance, increasing the concentration of Gd reduces the adhesion strength and hardness in the case of Gd-DLC coatings. Therefore, in this study, thin films with a low concentration of doping elements were chosen.

Table 2. Elemental composition, acquired from Rutherford backscattering spectrometry (RBS)-elastic recoil detection (ERD), where the remaining at. % is carbon.

Sample	Chemical Composition (at. %)		
	H	**Ar**	**Gd or Eu**
DLC	6.5	3.6	0
Gd-DLC	5.8	4.3	1.7
Eu-DLC	8	3.4	1.7

3.2. Scratch Test

Figure 4 shows the morphology of the scratches on the films designating the critical scratch load of LC1. LC1 denotes the beginning of coating cracking, which indicates cohesive failure [2]. As only conformal cracking was found, all samples exhibited proper thin-film adherence [4]. DLC structural and morphological characterization can also assist in understanding the differences in film adherence observed in films doped with various concentrations of doping elements. Higher sp^3/sp^2 ratios and densities have been reported to increase the adhesion of the film on the substrate [4,53]; however, the doping process has been shown to reduce the sp^3/sp^2 ratio, which affects the adhesion of the film [4,54]. Consistent with the findings of increased hardness and a decreased Young modulus, the Gd-DLC film containing 1.7 atomic percent of Gd exhibited the greatest critical load value, which is a representation of the better adherence of the film to the substrate.
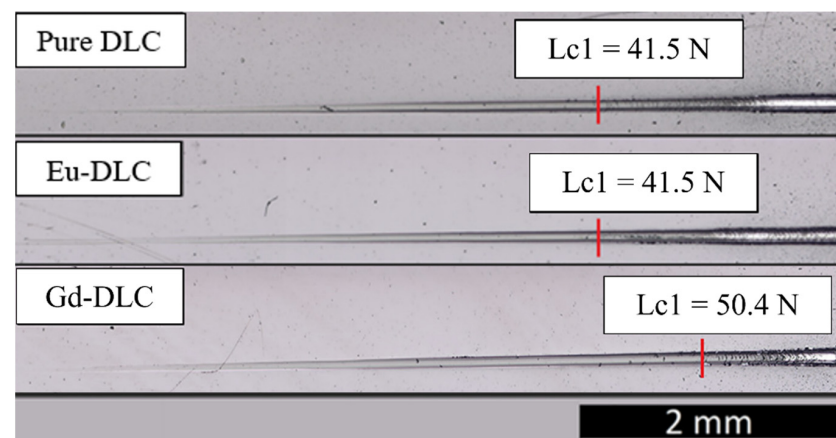
Figure 4. Scratch morphology of DLC films under increasing loads between 0 and 60 N.

3.3. Lubricant Viscosity

As previously stated, the Hersey parameter changes in the tested lubricant–thin film pairs in the current study were caused by velocity variations, not by the viscosity of the lubricant, because the experiments were performed at room temperature. Table 3 shows the measurement results for the viscosity of the used lubricant. The results indicate that the use of this ionic liquid as an additive for PAO 8 did not change the viscosity significantly. The viscosity of Newtonian liquids is regarded as a transition element in the Stribeck curve. In the experiments performed in this study, when the viscosity increased, the lubrication regime shifted toward the hydrodynamic regime, and thus the film thickness was increased at the same sliding speed compared to PAO 8 without additives.

Table 3. Viscosity values for the different lubricants at room temperature.

Lubricant	Dynamic Viscosity (mPa·s)	Kinematic Viscosity (mm²/s)
PAO 8	71.89	86.48
PAO 8 + IL (1 wt.%)	75.46	90.78

3.4. Stribeck Curves

Stribeck curves are presented as the coefficient of friction vs. the Hersey parameter or lambda ratio (λ). The Hersey parameter is a dimensionless number equal to the dynamic viscosity of the lubricant (η) times the velocity (u), divided by the normal load (P) per unit of contact length. Because the velocity was the only variable in these experiments, in this study, the values of the Hersey parameter shifted only through the velocity. The load was always approximately 25 N during the experiments, although the ring was aligned with a comparator [55]. This was because of the residual misalignment of the ring, which could not be avoided due to the dynamic nature of the rotating cylinder, but the variation was very small; therefore, the load was assumed to be constant with an insignificant error.

Figure 5 presents the Stribeck curves obtained from the test results at different sliding speeds for the DLC coatings. Based on these curves, three lubrication regimes can be found: boundary, mixed, and hydrodynamic lubrication (boundary lubrication, λ < 1; mixed lubrication, 1 < λ < 3; elastohydrodynamic lubrication, 3 < λ < 5; and hydrodynamic lubrication, λ > 5.).
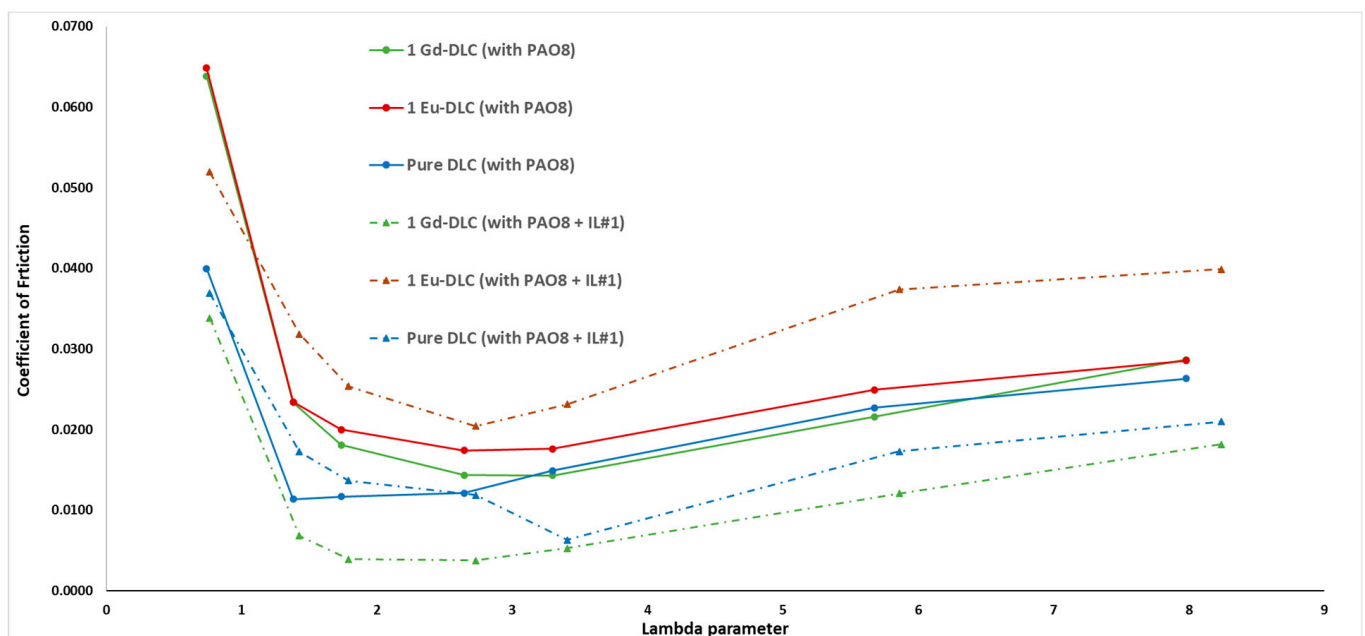
Figure 5. Stribeck curves obtained from the block-on-ring tribometer for PAO 8 and PAO 8 mixed with an IL for different lubricated surfaces.

The Stribeck curve graphically displays four regions on a horizontal axis, each with a corresponding slope that demonstrates a change in the coefficient of friction on the vertical axis. These regions are classified into four types of lubrication regimes: boundary, mixed, elastohydrodynamic, and hydrodynamic lubrication [56,57].

The boundary lubrication (BL) regime (λ < 1) is characterized by the support of the load through the microscopic asperities on the surface, where there is no continuous lubricant film. The sliding of asperities against each other can result in significant friction and wear, which can shorten the system's lifespan [56,58–60].

The mixed lubrication (ML) regime (1 < λ < 3) plays a significant role in internal combustion engines. It involves a combination of elastohydrodynamic lubrication and boundary lubrication characteristics. This implies that while some portions of the contact area are covered with a lubricant film, in other areas, the peak asperities of the moving surfaces slide against each other because there is no separating liquid film. Mixed lubrication is present in many engine components, such as piston rings, cams, and engine bearings. Understanding mixed lubrication is crucial for system engineers due to the fact that it is the most challenging lubrication regime in which to accurately predict friction. This

challenge is due to the complex interaction between surface topography and the oil film thickness [56,61,62].

The elastohydrodynamic lubrication (EL) regime ($3 < \lambda < 5$) is an extension of hydrodynamic lubrication that considers the deformation of the surfaces in contact. The film thickness in the EL regime is significantly lower than that in the hydrodynamic lubrication regime. As a result, an uninterrupted hydrodynamic film can only be maintained through the elastic deflection of the surfaces. Therefore, it is essential to consider these deflections when studying EHL [56,57].

In the hydrodynamic lubrication (HL) regime ($5 < \lambda$), the load is supported entirely by the lubricant film, and the asperities on the sliding surfaces are not in contact with each other. This is generally observed when the lambda ratio exceeds 5 [58,63].

In the EHL and HL regimes, as the speed increases, the lubricant film may not be able to keep up with the changes in pressure, and the lubricant may not have enough time to flow into the contact area and form a thick enough fluid film, leading to increased friction [64,65]. In addition, the viscosity of the lubricant typically decreases with increasing temperature, which can occasionally occur at very high sliding speeds due to the heat generated by friction.

When the Stribeck curves for different films were compared, it was discovered that, in general, adding the ionic liquid to the PAO 8 lubricant reduced the CoF at the lowest sliding speed achievable with the used tribometer, especially for the Gd-doped DLC film. The Eu-DLC film did not show a better performance compared with the pure DLC film in the presence of the IL. Before adding the IL, the doped DLC films (Eu-DLC and Gd-DLC) paired with pure PAO 8 did not present a good performance compared with the pure DLC film, but after adding 1 wt.% IL to PAO 8, the performance of the Gd-DLC film was even better than that of the pure DLC film in the boundary, mixed, elastohydrodynamic, and hydrodynamic lubrication regimes, which can be attributed to its better interaction with the ionic liquid additive. In the literature, two lubricating mechanisms supporting the use of ionic liquids as lubricant additives have been discussed. The formation of adsorbed layers is the first reason that has been mentioned. These layers have the ability to promote movement between two surfaces that are sliding against each other, owing to their low shear. The formation of a tribofilm on metal surfaces is the second reason that has been discussed. These protective layers are formed as a result of chemical reactions that occur between ionic liquids and the surfaces that are in contact with them during friction [2,66].

According to the suggested mechanism for adsorbed layers, the anionic component of ionic liquids is drawn towards the positively charged surface of metals, leading to surface adsorption [67]. The cationic component can then be adsorbed by another anionic entity, forming single- or multi-layered adsorbed structures on the surface. These structures create a film on the metal surface and have low interlayer strength, which helps to reduce friction and promote movement between the contacting surfaces [2,66,68,69].

Based on the obtained data from the viscosity measurements, the minimum film thickness (h_0) and lambda ratio (ratio of minimum film thickness to composite surface roughness) were calculated (Tables 4 and 5) using the Hamrock–Dowson equation [70].

Table 4. Characteristics of a lubricant film with PAO 8 based on the sliding speed of the cylinder (u is the speed of the ring). * Boundary lubrication = BL; mixed lubrication = ML; elastohydrodynamic lubrication = EL; hydrodynamic lubrication = HL.

u (m/s)	0.02	0.05	0.07	0.13	0.18	0.4	0.66
h0 (m)	3.5×10^{-8}	6.6×10^{-8}	8.3×10^{-8}	1.2×10^{-7}	1.5×10^{-7}	2.7×10^{-7}	3.8×10^{-7}
λ	0.74	1.38	1.73	2.65	3.30	5.68	7.98
Lubrication regime *	BL	ML	ML	ML	EL	HL	HL
Hersey parameter	8.1×10^{-7}	1.8×10^{-6}	2.9×10^{-6}	4.5×10^{-6}	6.2×10^{-6}	1.4×10^{-5}	2.3×10^{-5}

Table 5. Characteristics of a lubricant film with PAO 8 + 1 wt.% IL based on the sliding speed of the cylinder (u is the speed of the ring). * Boundary lubrication = BL; mixed lubrication = ML; elastohydrodynamic lubrication = EL; hydrodynamic lubrication = HL.

u (m/s)	0.02	0.05	0.07	0.13	0.18	0.4	0.66
h_0 (m)	3.7×10^{-8}	6.8×10^{-8}	8.6×10^{-8}	1.3×10^{-7}	1.6×10^{-7}	2.8×10^{-7}	4.0×10^{-7}
λ	0.76	1.42	1.79	2.73	3.40	5.86	8.24
Lubrication regime *	BL	ML	ML	ML	EL	HL	HL
Hersey parameter	8.5×10^{-7}	1.9×10^{-6}	2.9×10^{-6}	4.7×10^{-6}	6.6×10^{-6}	1.5×10^{-5}	2.4×10^{-5}

Tables 4 and 5 show the lambda ratio (λ), which is an indicator of the lubricant regime in an operating contact. For both lubricants, the lubrication regime starts with the fully hydrodynamic regime, and as the sliding speed decreases, the lambda ratio also decreases; finally, the lubrication regime completely changes to the boundary lubrication regime, and the surfaces of the block and ring come into contact, which can cause wear on both surfaces. However, as the viscosity of PAO 8 + 1 wt.% is higher than that of PAO 8, the film thickness is higher for this case, and the whole curve shifts to the right slightly.
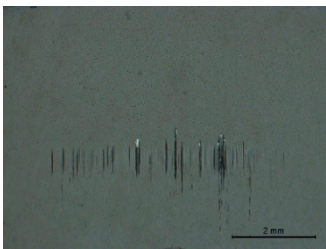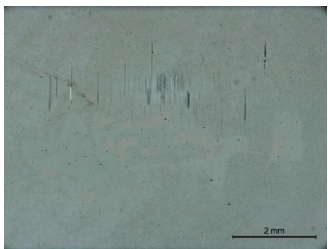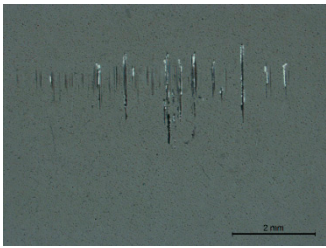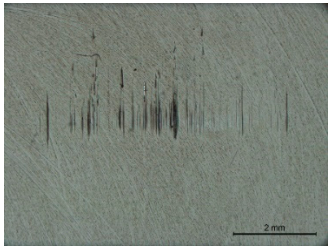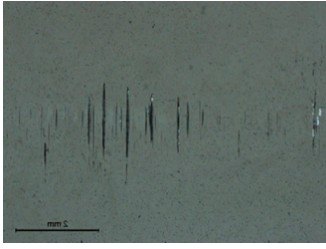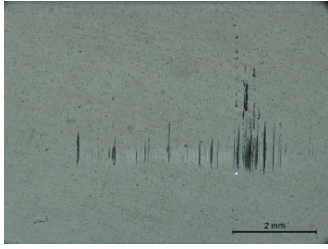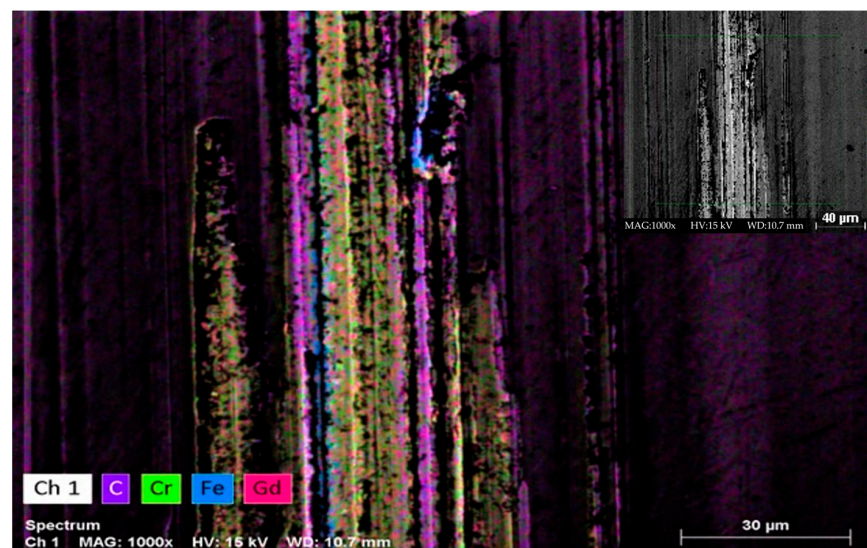
3.5. Wear Analysis

Optical microscopy (OM) was used to evaluate the wear of the coatings after the tribology tests. Because quantifying the wear of DLC coatings is difficult (since they have high wear resistance), wear track images captured using an optical microscope were qualitatively compared [55]. Based on the obtained results (Table 6), the introduction of the IL as an additive to PAO 8 decreased wear in comparison with pure PAO 8 paired with the Gd-DLC and pure DLC coatings. However, for the Eu-DLC coating, it is difficult to draw the same conclusion, as the images for this coating paired with PAO 8 and PAO8 + 1 wt. % are hard to compare. In addition, comparing the three films lubricated with 1 wt.% of IL is not an easy task based on the obtained images, since they look quite similar. As presented in Tables 4 and 5, the lubrication regime is the boundary or mixed regime at the lower sliding speeds, which can lead to surface–surface contact, eventually leading to wear on both surfaces.
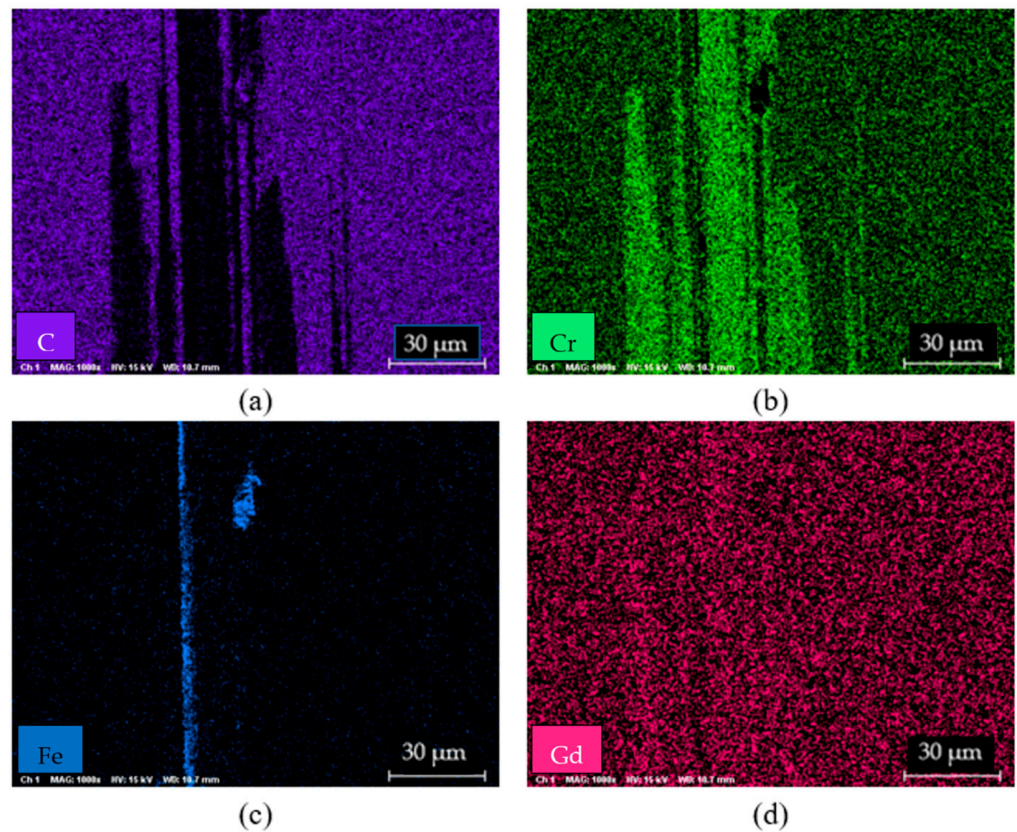
3.6. SEM/EDS Analysis

SEM-EDS was used to evaluate the effect of using the IL as an additive on the DLC thin films, but this technique could not efficiently detect the formation of a tribofilm in this case; therefore, it would be preferable to use more surface-sensitive characterization techniques such as time-of-flight secondary-ion mass spectrometry (ToF-SIMS) or neutron reflectometry analysis to recognize the presence of a tribofilm. Figures 6–9 show the elemental maps of the areas selected on the Gd-DLC and Eu-DLC films. As can be seen, the thin film was removed in some sections, and the chromium element of the interlayer was detected. Iron was also detected in both the Gd-DLC and Eu-DLC films, which may have been due to adhesive wear from the steel ring, or it may have come from the substrate of the thin film due to abrasive wear.

**Table 6.** Optical microscopy images of different lubricant films.

Pure DLC	
(**a**) PAO 8	(**b**) PAO 8 + IL

Gd-DLC	
(**a**) PAO 8	(**b**) PAO 8 + IL

Eu-DLC	
(**a**) PAO 8	(**b**) PAO 8 + IL

Figure 6. Elemental analysis of the surface of the Gd-DLC film paired with PAO 8 + 1 wt. % IL using EDS. The image in the right upper corner shows the SEM micrograph of the surface without presenting elements.

Figure 7. Element mapping of the Gd-DLC thin film paired with PAO 8 + 1 wt. % IL after the tribology test: (**a**) carbon; (**b**) chromium; (**c**) iron; (**d**) gadolinium (obtained through SEM/EDS characterization).
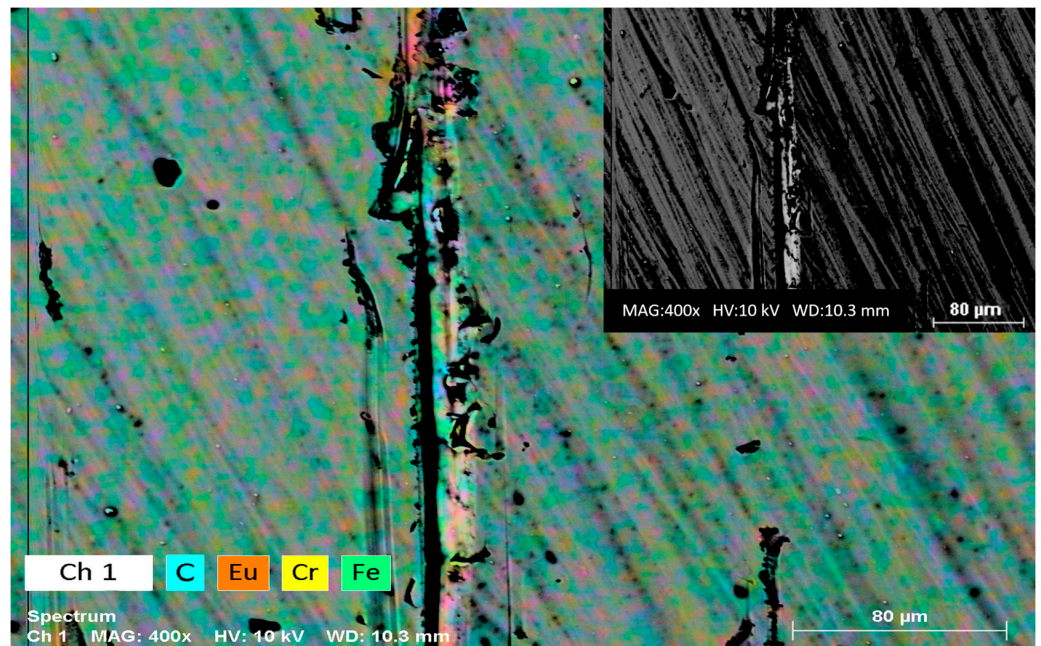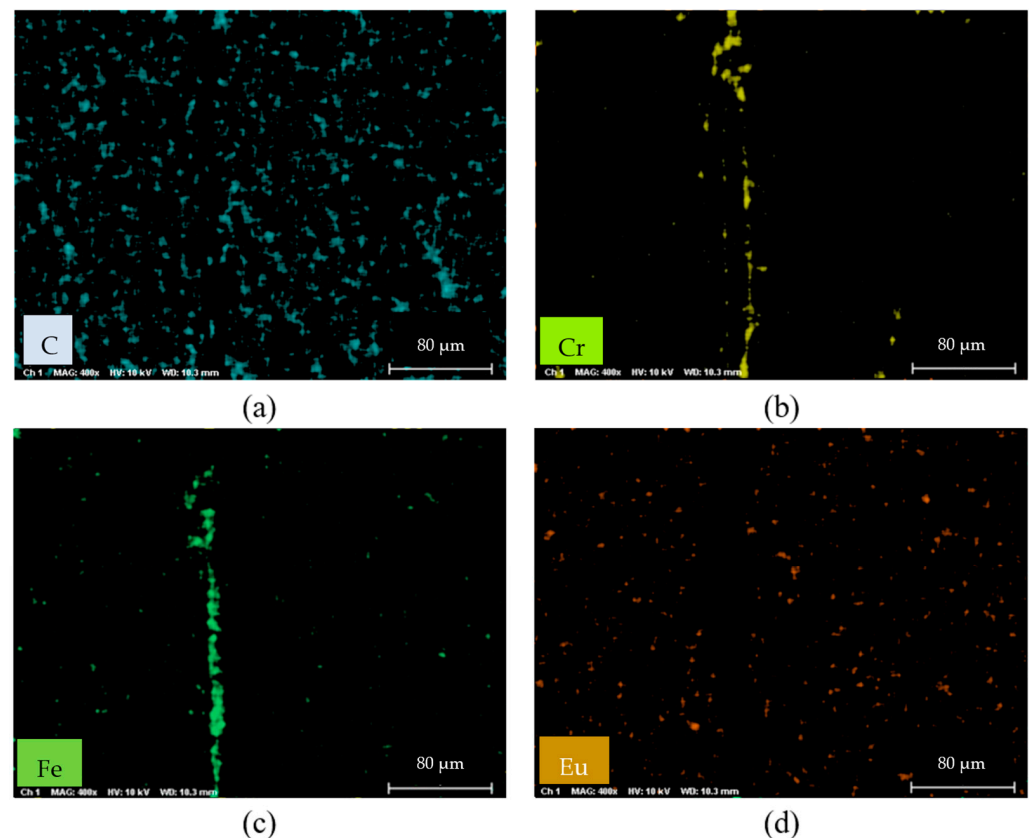

Figure 8. Elemental analysis of the surface of the Eu-DLC film paired with PAO 8 + 1 wt.% IL using EDS. The image in the right upper corner shows the SEM micrograph of the surface without presenting elements.

Figure 9. Element mapping of the Eu-DLC thin film paired with PAO 8 + 1 wt.% IL after the tribology test: (**a**) carbon; (**b**) chromium; (**c**) iron; (**d**) europium (obtained through SEM/EDS characterization).

4. Conclusions

In the present study, the effect of adding 1 wt.% $[P_{66614}][DEHP]$ ionic liquid additive to PAO 8 for the lubricated sliding pairs of AISI 3415 steel and three types of DLC coatings (Gd-DLC, Eu-DLC, and pure DLC coatings) was studied. The Gd-DLC coating had the highest hardness among these coatings and, according to the scratch measurements (critical load value), the best adherence to the substrate. The best interaction with the IL and a significant CoF reduction in all lubrication regimes were obtained with the Gd-DLC coating. For the Eu-DLC coating paired with PAO 8 + 1 wt.% IL as an additive, a reduction in friction occurred in the boundary lubrication regime in comparison to the Eu-DLC coating paired with PAO 8. For the pure DLC coating paired with PAO 8 + 1 wt.% IL as an additive, a reduction in the CoF occurred in the boundary, elastohydrodynamic, and hydrodynamic lubrication regimes compared with the pure DLC coating paired with PAO 8. The wear results could not be quantitatively measured; however, the qualitative approach showed that adding an IL to the lubricated contact decreased the wear on the Gd-DLC and pure DLC coatings. Nevertheless, a comparison of wear among these coatings is not feasible based on the available techniques for wear quantification.

Author Contributions: Conceptualization, F.F. (Fábio Ferreira) and A.R.; methodology, F.F. (Fábio Ferreira) and A.R.; formal analysis, M.S., T.O. and L.V.; investigation, M.S. and L.V.; resources, F.F. (Fábio Ferreira) and A.R.; writing—original draft preparation, M.S. and F.F. (Filipe Fernandes); writing—review and editing, F.F. (Fábio Ferreira), T.O. and L.V.; supervision, F.F. (Fábio Ferreira) and F.F. (Filipe Fernandes); project administration, F.F. (Fábio Ferreira) and F.F. (Filipe Fernandes); funding acquisition, F.F. (Fábio Ferreira). All authors have read and agreed to the published version of the manuscript.

Institutional Review Board Statement: Not applicable.

Informed Consent Statement: Not applicable.

Data Availability Statement: The data presented in this study are available on request from the corresponding author.

Conflicts of Interest: The authors declare no conflict of interest.

References

1.　Holmberg, K.; Erdemir, A. The Impact of Tribology on Energy Use and CO_2 Emission Globally and in Combustion Engine and Electric Cars. *Tribol. Int.* **2019**, *135*, 389–396. [CrossRef]

2.　Khanmohammadi, H.; Wijanarko, W.; Cruz, S.; Evaristo, M.; Espallargas, N. Triboelectrochemical Friction Control of W- and Ag-Doped DLC Coatings in Water-Glycol with Ionic Liquids as Lubricant Additives. *RSC Adv.* **2022**, *12*, 3573–3583. [CrossRef] [PubMed]

3.　Zichao, L.; Bin, S.; Fanghong, S.; Zhiming, Z.; Songshou, G. Diamond-Coated Tube Drawing Die Optimization Using Finite Element Model Simulation and Response Surface Methodology. *Proc. Inst. Mech. Eng. J. Eng. Manuf.* **2014**, *228*, 1432–1441. [CrossRef]

4.　Fontes, M.A.; Serra, R.G.H.; Fernandes, F.D.; Cavaleiro Rodrigues de Carvalho, A.A.; de Sousa Ferreira, F.E. Comparison of Mechanical and Tribological Properties of Diamond-like Carbon Coatings Doped with Europium and Gadolinium Produced by HiPIMS. *Proc. Inst. Mech. Eng. J. Eng. Manuf.* **2022**, 237. [CrossRef]

5.　Zeng, Q.; Ning, Z. High-Temperature Tribological Properties of Diamond-like Carbon Films: A Review. *Rev. Adv. Mater. Sci.* **2021**, *60*, 276–292. [CrossRef]

6.　Sánchez-López, J.C.; Fernández, A. Doping and Alloying Effects on DLC Coatings. In *Tribology of Diamond-like Carbon Films: Fundamentals and Applications*; Donnet, C., Erdemir, A., Eds.; Springer US: Boston, MA, USA, 2008; pp. 311–338. ISBN 978-0-387-49891-1.

7.　Zhao, F.; Li, H.; Ji, L.; Wang, Y.; Zhou, H.; Chen, J. Ti-DLC Films with Superior Friction Performance. *Diam. Relat. Mater.* **2010**, *19*, 342–349. [CrossRef]

8.　Ming, M.Y.; Jiang, X.; Piliptsou, D.G.; Zhuang, Y.; van Rogachev, A.; Rudenkov, A.S.; Balmakou, A. Chromium-Modified a-C Films with Advanced Structural, Mechanical and Corrosive-Resistant Characteristics. *Appl. Surf. Sci.* **2016**, *379*, 424–432. [CrossRef]

9.　Balestra, R.M.; Castro, A.M.G.; Evaristo, M.; Escudeiro, A.; Mutafov, P.; Polcar, T.; Cavaleiro, A. Carbon-Based Coatings Doped by Copper: Tribological and Mechanical Behavior in Olive Oil Lubrication. *Surf. Coat. Technol.* **2011**, *205*, S79–S83. [CrossRef]

10.　Bhowmick, S.; Banerji, A.; Alpas, A.T. Tribological Behaviour of W-DLC against an Aluminium Alloy Subjected to Lubricated Sliding. *Tribol. Ind.* **2015**, *37*, 277–283.

11.　Bociaga, D.; Komorowski, P.; Batory, D.; Szymanski, W.; Olejnik, A.; Jastrzebski, K.; Jakubowski, W. Silver-Doped Nanocomposite Carbon Coatings (Ag-DLC) for Biomedical Applications—Physiochemical and Biological Evaluation. *Appl. Surf. Sci.* **2015**, *355*, 388–397. [CrossRef]

12.　Evaristo, M.; Polcar, T.; Cavaleiro, A. Tribological Behaviour of W-Alloyed Carbon-Based Coatings in Dry and Lubricated Sliding Contact. *Lubr. Sci.* **2014**, *26*, 428–439. [CrossRef]

13.　Evaristo, M.; Fernandes, F.; Cavaleiro, A. Room and High Temperature Tribological Behaviour of W-DLC Coatings Produced by DCMS and Hybrid DCMS-HiPIMS Configuration. *Coatings* **2020**, *10*, 319. [CrossRef]

14.　Wongpanya, P.; Silawong, P.; Photongkam, P. Adhesion and Corrosion of Al–N Doped Diamond-like Carbon Films Synthesized by Filtered Cathodic Vacuum Arc Deposition. *Ceram. Int.* **2022**, *48*, 20743–20759. [CrossRef]

15.　Santiago, J.A.; Fernández-Martínez, I.; Sánchez-López, J.C.; Rojas, T.C.; Wennberg, A.; Bellido-González, V.; Molina-Aldareguia, J.M.; Monclús, M.A.; González-Arrabal, R. Tribomechanical Properties of Hard Cr-Doped DLC Coatings Deposited by Low-Frequency HiPIMS. *Surf. Coat. Technol.* **2020**, *382*, 124899. [CrossRef]

16.　Wongpanya, P.; Silawong, P.; Photongkam, P. Nanomechanical Properties and Thermal Stability of Al–N-Co-Doped DLC Films Prepared by Filtered Cathodic Vacuum Arc Deposition. *Surf. Coat. Technol.* **2021**, *424*, 127655. [CrossRef]

17.　Ding, J.C.; Dai, W.; Zhang, T.F.; Zhao, P.; Yun, J.M.; Kim, K.H.; Wang, Q.M. Microstructure and Properties of Nb-Doped Diamond-like Carbon Films Deposited by High Power Impulse Magnetron Sputtering. *Thin Solid Film.* **2018**, *663*, 159–167. [CrossRef]

18.　Stoy, L.; Xu, J.; Kulkarni, Y.; Huang, C.-H. Ionic Liquid Recovery of Rare-Earth Elements from Coal Fly Ash: Process Efficiency and Sustainability Evaluations. *ACS Sustain. Chem. Eng.* **2022**, *10*, 11824–11834. [CrossRef]

19.　Mishra, B.B.; Devi, N. Application of Bifunctional Ionic Liquids for Extraction and Separation of Eu3+ from Chloride Medium. *Trans. Nonferrous Met. Soc. China* **2022**, *32*, 2061–2070. [CrossRef]

20. Zhou, F.; Liang, Y.; Liu, W. Ionic Liquid Lubricants: Designed Chemistry for Engineering Applications. *Chem. Soc. Rev.* **2009**, *38*, 2590–2599. [CrossRef]
21. Ye, C.; Liu, W.; Chen, Y.; Yu, L. Room-Temperature Ionic Liquids: A Novel Versatile Lubricant. *Chem. Commun.* **2001**, *21*, 2244–2245. [CrossRef]
22. Chen, Y.; Renner, P.; Liang, H. A Review of Current Understanding in Tribochemical Reactions Involving Lubricant Additives. *Friction* **2022**, *11*, 489–512. [CrossRef]
23. Zhou, Y.; Leonard, D.N.; Guo, W.; Qu, J. Understanding Tribofilm Formation Mechanisms in Ionic Liquid Lubrication. *Sci. Rep.* **2017**, *7*, 8426. [CrossRef]
24. Barnhill, W.C.; Qu, J.; Luo, H.; Meyer, H.M.; Ma, C.; Chi, M.; Papke, B.L. Phosphonium-Organophosphate Ionic Liquids as Lubricant Additives: Effects of Cation Structure on Physicochemical and Tribological Characteristics. *ACS Appl. Mater. Interfaces* **2014**, *6*, 22585–22593. [CrossRef] [PubMed]
25. Yu, B.; Bansal, D.G.; Qu, J.; Sun, X.; Luo, H.; Dai, S.; Blau, P.J.; Bunting, B.G.; Mordukhovich, G.; Smolenski, D.J. Oil-Miscible and Non-Corrosive Phosphonium-Based Ionic Liquids as Candidate Lubricant Additives. *Wear* **2012**, *289*, 58–64. [CrossRef]
26. Qu, J.; Bansal, D.G.; Yu, B.; Howe, J.Y.; Luo, H.; Dai, S.; Li, H.; Blau, P.J.; Bunting, B.G.; Mordukhovich, G.; et al. Antiwear Performance and Mechanism of an Oil-Miscible Ionic Liquid as a Lubricant Additive. *ACS Appl. Mater. Interfaces* **2012**, *4*, 997–1002. [CrossRef] [PubMed]
27. Otero, I.; López, E.R.; Reichelt, M.; Villanueva, M.; Salgado, J.; Fernández, J. Ionic Liquids Based on Phosphonium Cations As Neat Lubricants or Lubricant Additives for a Steel/Steel Contact. *ACS Appl. Mater. Interfaces* **2014**, *6*, 13115–13128. [CrossRef] [PubMed]
28. Somers, A.E.; Khemchandani, B.; Howlett, P.C.; Sun, J.; MacFarlane, D.R.; Forsyth, M. Ionic Liquids as Antiwear Additives in Base Oils: Influence of Structure on Miscibility and Antiwear Performance for Steel on Aluminum. *ACS Appl. Mater. Interfaces* **2013**, *5*, 11544–11553. [CrossRef]
29. Milewski, K.; Kudliński, J.; Madej, M.; Ozimina, D.; Kudliński-Trzuskawica, J.; Madej, P.M. The Interaction between Diamond-like Carbon (Dlc) Coatings and Ionic Liquids under Boundary Lubrication Conditions. *Metalurgija* **2017**, *56*, 55–58.
30. González, R.; Battez, A.H.; Viesca, J.L.; Higuera-Garrido, A.; Fernández-González, A. Lubrication of DLC Coatings with Two Tris(Pentafluoroethyl)Trifluorophosphate Anion-Based Ionic Liquids. *Tribol. Trans.* **2013**, *56*, 887–895. [CrossRef]
31. Shahid Arshad, M.; Čoga, L.; Geue, T.; Kovač, J.; Cruz, S.M.A.; Kalin, M. The W-cluster reactive sites interaction model for WDLC coatings with ionic liquids. *Tribol. Int.* **2023**, *185*, 108550. [CrossRef]
32. Arshad, M.S.; Kovač, J.; Cruz, S.; Kalin, M. Physicochemical and Tribological Characterizations of WDLC Coatings and Ionic-Liquid Lubricant Additives: Potential Candidates for Low Friction under Boundary-Lubrication Conditions. *Tribol. Int.* **2020**, *151*, 106482. [CrossRef]
33. Forsberg, P.; Gustavsson, F.; Renman, V.; Hieke, A.; Jacobson, S. Performance of DLC Coatings in Heated Commercial Engine Oils. *Wear* **2013**, *304*, 211–222. [CrossRef]
34. Vahidi, A.; Fonseca, D.; Oliveira, J.; Cavaleiro, A.; Ramalho, A.; Ferreira, F. Advanced Tribological Characterization of Dlc Coatings Produced by Ne-Hipims for the Application on the Piston Rings of Internal Combustion Engines. *Appl. Sci.* **2021**, *11*, 10498. [CrossRef]
35. Kowalczyk, J.; Kulczycki, A.; Madej, M.; Ozimina, D. Effect of ZDDP and Fullerenes Added to PAO 8 Lubricant on Tribological Properties of the Surface Layer of Steel Bare Steel and W-DLC Coating. *Tribologia* **2022**, *299*, 19–32. [CrossRef]
36. Turanov, A.N.; Karandashev, V.K.; Boltoeva, M. Solvent Extraction of Intra-Lanthanides Using a Mixture of TBP and TODGA in Ionic Liquid. *Hydrometallurgy* **2020**, *195*, 105367. [CrossRef]
37. Bolander, N.W.; Steenwyk, B.D.; Sadeghi, F.; Gerber, G.R. Lubrication Regime Transitions at the Piston Ring-Cylinder Liner Interface. *Proc. Inst. Mech. Eng. J. Eng. Tribol.* **2005**, *219*, 19–31. [CrossRef]
38. Pusterhofer, M.; Summer, F.; Wuketich, D.; Grün, F. Development of a Model Test System for a Piston Ring/Cylinder Liner-Contact with Focus on near-to-Application Seizure Behaviour. *Lubricants* **2019**, *7*, 104. [CrossRef]
39. Hu, Z. Chapter 6—Characterization of Materials, Nanomaterials, and Thin Films by Nanoindentation. In *Microscopy Methods in Nanomaterials Characterization*; Thomas, S., Thomas, R., Zachariah, A.K., Mishra, R.K., Eds.; Elsevier: Amsterdam, The Netherlands, 2017; pp. 165–239. ISBN 978-0-323-46141-2.
40. Sharma, S. Tribological Behaviour of Laser Treated C-Alloyed Tmd Coatings in Rubber Contact Effects of Protein on Tribocorrosion Behavior of Ti-6Al-4V. Master's Dissertation, University of Coimbra, Coimbra, Portugal, 2021.
41. Zhou, X.; Tunmee, S.; Suzuki, T.; Phothongkam, P.; Kanda, K.; Komatsu, K.; Kawahara, S.; Ito, H.; Saitoh, H. Quantitative NEXAFS and Solid-State NMR Studies of Sp3/(Sp2+sp3) Ratio in the Hydrogenated DLC Films. *Diam. Relat. Mater.* **2017**, *73*, 232–240. [CrossRef]
42. Barradas, N.P.; Jeynes, C.; Webb, R.P. Simulated Annealing Analysis of Rutherford Backscattering Data. *Appl. Phys. Lett.* **1998**, *71*, 291. [CrossRef]
43. Gurbich, A.F. SigmaCalc Recent Development and Present Status of the Evaluated Cross-Sections for IBA. *Nucl. Instrum. Methods Phys. Res.* **2016**, *371*, 27–32. [CrossRef]
44. Luo, Q. Electron Microscopy and Spectroscopy in the Analysis of Friction and Wear Mechanisms. *Lubricants* **2018**, *6*, 58. [CrossRef]
45. Vetter, J. 60years of DLC Coatings: Historical Highlights and Technical Review of Cathodic Arc Processes to Synthesize Various DLC Types, and Their Evolution for Industrial Applications. *Surf. Coat. Technol.* **2014**, *257*, 213–240. [CrossRef]

46. Liu, Y.; Erdemir, A.; Meletis, E.I. A Study of the Wear Mechanism of Diamond-like Carbon Films. *Surf. Coat. Technol.* **1996**, *82*, 48–56. [CrossRef]

47. Robertson, J. Diamond-like Amorphous Carbon. *Mater. Sci. Eng. R Rep.* **2002**, *37*, 129–281. [CrossRef]

48. Grill, A. Diamond-like Carbon: State of the Art. *Diam. Relat. Mater.* **1999**, *8*, 428–434. [CrossRef]

49. Ding, J.C.; Mei, H.; Jeong, S.; Zheng, J.; Wang, Q.M.; Kim, K.H. Effect of Bias Voltage on the Microstructure and Properties of Nb-DLC Films Prepared by a Hybrid Sputtering System. *J. Alloys Compd.* **2021**, *861*, 158505. [CrossRef]

50. Ding, J.C.; Chen, M.; Mei, H.; Jeong, S.; Zheng, J.; Yang, Y.; Wang, Q.; Kim, K.H. Microstructure, Mechanical, and Wettability Properties of Al-Doped Diamond-like Films Deposited Using a Hybrid Deposition Technique: Bias Voltage Effects. *Diam. Relat. Mater.* **2022**, *123*, 108861. [CrossRef]

51. Matthews, A.; Franklin, S.; Holmberg, K. Tribological Coatings: Contact Mechanisms and Selection. *J. Phys. Appl. Phys.* **2007**, *40*, 5463–5475. [CrossRef]

52. Cao, L.; Liu, J.; Wan, Y.; Pu, J. Corrosion and Tribocorrosion Behavior of W Doped DLC Coating in Artificial Seawater. *Diam. Relat. Mater.* **2020**, *109*, 108019. [CrossRef]

53. Kashyap, A.; Harsha, A.P.; Kondaiah, P.; Barshilia, H.C. Study on Galling Behaviour of HiPIMS Deposited Mo/DLC Multilayer Coatings at Ambient and Elevated Temperature. *Wear* **2022**, *498–499*, 204327. [CrossRef]

54. Konkhunthot, N.; Photongkam, P.; Wongpanya, P. Improvement of Thermal Stability, Adhesion Strength and Corrosion Performance of Diamond-like Carbon Films with Titanium Doping. *Appl. Surf. Sci.* **2019**, *469*, 471–486. [CrossRef]

55. Cardoso, F.; Ferreira, F.; Cavaleiro, A.; Ramalho, A. Performance of Diamond-like Carbon Coatings (Produced by the Innovative Ne-HiPIMS Technology) under Different Lubrication Regimes. *Wear* **2021**, *477*, 203775. [CrossRef]

56. Wang, Y.; Wang, Q.J. Stribeck Curves. In *Encyclopedia of Tribology*; Wang, Q.J., Chung, Y.-W., Eds.; Springer US: Boston, MA, USA, 2013; pp. 3365–3370. ISBN 978-0-387-92897-5.

57. Marinescu, I.D.; Rowe, W.B.; Dimitrov, B.; Inasaki, I. Process Fluids for Abrasive Machining. In *Tribology of Abrasive Machining Processes*; Marinescu, I.D., Rowe, W.B., Dimitrov, B., Inasaki, I., Eds.; William Andrew Publishing: Norwich, NY, USA, 2004; pp. 531–585. ISBN 978-0-8155-1490-9.

58. Kalin, M.; Velkavrh, I.; Vižintin, J. The Stribeck Curve and Lubrication Design for Non-Fully Wetted Surfaces. *Wear* **2009**, *267*, 1232–1240. [CrossRef]

59. Wang, Y.; Wang, Q.J.; Lin, C.; Shi, F. Development of a Set of Stribeck Curves for Conformal Contacts of Rough Surfaces. *Tribol. Trans.* **2006**, *49*, 526–535. [CrossRef]

60. Lu, X.; Khonsari, M.M.; Gelinck, E.R.M. The Stribeck Curve: Experimental Results and Theoretical Prediction. *J. Tribol.* **2006**, *128*, 789–794. [CrossRef]

61. Martini, A.; Zhu, D.; Wang, Q. Friction Reduction in Mixed Lubrication. *Tribol. Lett.* **2007**, *28*, 139–147. [CrossRef]

62. Xin, Q. Friction and Lubrication in Diesel Engine System Design. In *Diesel Engine System Design*; Xin, Q., Ed.; Woodhead Publishing: Thorston, UK, 2013; pp. 651–758. ISBN 978-1-84569-715-0.

63. Li, P.; Zhang, F.; Zhang, H.; Wang, T.; Wang, Q.; Qiao, W. Lubrication Performance of Kite-Shaped Microtexture under Hydrodynamic Lubrication. *Tribol. Int.* **2023**, *179*, 108144. [CrossRef]

64. Linjamaa, A.; Lehtovaara, A.; Kallio, M.; Léger, A. Running-in Effects on Friction of Journal Bearings under Slow Sliding Speeds. *Proc. Inst. Mech. Eng. J. Eng. Tribol.* **2019**, *234*, 362–372. [CrossRef]

65. Kalin, M.; Velkavrh, I. Non-Conventional Inverse-Stribeck-Curve Behaviour and Other Characteristics of DLC Coatings in All Lubrication Regimes. *Wear* **2013**, *297*, 911–918. [CrossRef]

66. Xiao, H. Ionic Liquid Lubricants: Basics and Applications. *Tribol. Trans.* **2017**, *60*, 20–30. [CrossRef]

67. Kajdas, C. Importance of Anionic Reactive Intermediates for Lubricant Component Reactions with Friction Surfaces. *Lubr. Sci.* **1994**, *6*, 203–228. [CrossRef]

68. Atkin, R.; el Abedin, S.Z.; Hayes, R.; Gasparotto, L.H.S.; Borisenko, N.; Endres, F. AFM and STM Studies on the Surface Interaction of [BMP]TFSA and [EMIm]TFSA Ionic Liquids with Au(111). *J. Phys. Chem.* **2009**, *113*, 13266–13272. [CrossRef]

69. Perkin, S.; Albrecht, T.; Klein, J. Layering and Shear Properties of an Ionic Liquid, 1-Ethyl-3-Methylimidazolium Ethylsulfate, Confined to Nano-Films between Mica Surfaces. *Phys. Chem. Chem. Phys.* **2010**, *12*, 1243–1247. [CrossRef] [PubMed]

70. Lubrecht, A.A.; Venner, C.H.; Colin, F. Film Thickness Calculation in Elasto-Hydrodynamic Lubricated Line and Elliptical Contacts: The Dowson, Higginson, Hamrock Contribution. *Proc. Inst. Mech. Eng. J. Eng. Tribol.* **2009**, *223*, 511–515. [CrossRef]